IJMMM International Journal of Minerals, Metallurgy and Materials 矿物冶金与材料学报（英文版）

Preparation of FeCoNi medium entropy alloy from Fe^{3+}–Co^{2+}–Ni^{2+} solution system

Zongyou Cheng, Qing Zhao, Mengjie Tao, Jijun Du, Xingxi Huang, and Chengjun Liu

Cite this article as:
Zongyou Cheng, Qing Zhao, Mengjie Tao, Jijun Du, Xingxi Huang, and Chengjun Liu, Preparation of FeCoNi medium entropy alloy from Fe^{3+}–Co^{2+}–Ni^{2+} solution system, *Int. J. Miner. Metall. Mater.*, 32(2025), No. 1, pp. 92-101. https://doi.org/10.1007/s12613-024-2888-6

INTERNATIONAL JOURNAL OF
Minerals, Metallurgy and Materials

Volume 32, Number 1, January 2025
Page 92

Research Article https://doi.org/10.1007/s12613-024-2888-6

Preparation of FeCoNi medium entropy alloy from Fe^{3+}–Co^{2+}–Ni^{2+} solution system

Zongyou Cheng[1,2], *Qing Zhao*[1,2,3)✉], *Mengjie Tao*[1,2)✉], *Jijun Du*[1,2)], *Xingxi Huang*[1,2)], *and Chengjun Liu*[1,2)]

1) Key Laboratory for Ecological Metallurgy of Multimetallic Mineral (Ministry of Education), Northeastern University, Shenyang 110819, China
2) School of Metallurgy, Northeastern University, Shenyang 110819, China
3) Engineering Research Center of Frontier Technologies for Low-carbon Steelmaking (Ministry of Education), Shenyang 110819, China
(Received: 18 December 2023; revised: 15 March 2024; accepted: 20 March 2024)

Abstract: In recent years, medium entropy alloys have become a research hotspot due to their excellent physical and chemical performances. By controlling reasonable elemental composition and processing parameters, the medium entropy alloys can exhibit similar properties to high entropy alloys and have lower costs. In this paper, a FeCoNi medium entropy alloy precursor was prepared via sol–gel and co-precipitation methods, respectively, and FeCoNi medium entropy alloys were prepared by carbothermal and hydrogen reduction. The phases and magnetic properties of FeCoNi medium entropy alloy were investigated. Results showed that FeCoNi medium entropy alloy was produced by carbothermal and hydrogen reduction at 1500°C. Some carbon was detected in the FeCoNi medium entropy alloy prepared by carbothermal reduction. The alloy prepared by hydrogen reduction was uniform and showed a relatively high purity. Moreover, the hydrogen reduction product exhibited better saturation magnetization and lower coercivity.

Keywords: medium entropy alloy; sol–gel; co-precipitation; carbothermal; hydrogen reduction

1. Introduction

In recent years, the high entropy alloy (HEA) has received extensive attention in advanced materials science [1–3]. The key effects of HEA include high entropy effect, sluggish diffusion, severe lattice distortion, and cocktail effect [4–5]. Medium entropy alloy (MEA) is a kind of alloy system between traditional alloy (low entropy alloy) and HEA, which commonly contains less than four principal elements. The entropy of mixing of FeCoNi MEA is close to that of traditional alloy, while exhibiting excellent properties like HEA, such as high strength, high temperature softening resistance, high hardness [6–11], strong corrosion-resistance [12–14], and well electromagnetic properties [15–21], etc.

Magnetic materials refer to substances composed of transition elements such as Fe, Co, Ni, and their alloys that can directly or indirectly generate magnetism. Table 1 shows the magnetic properties of entropy alloy in FeCoNi system obtained by different preparation methods. In recent years, research has shown that FeCoNi MEA, as a soft magnetic material that is easy to magnetize and demagnetize, has broad application prospects in magnetic storage and ultra-high-density magnetic recording [15,22–23]. The methods for preparing FeCoNi MEA include chemical reduction [15–16], mechanical alloying [17–19], and vacuum melting [20–21]. The saturation magnetization of the products prepared by these methods was similar and showed a big gap in coercivity. It was reported that using the liquid phase method to prepare precursor was beneficial to control the element ratio, refine grain size, and reduce the costs [24–38]. Moreover, some Fe, Co, and Ni resources of waste can be recovered and utilized via this route [39–40].

Table 1. Magnetic properties of medium entropy alloys FeCoNi system [15–21]

No.	$Fe_xCo_yNi_z$	Method	M_s / (emu·g^{-1})	H_c / (A·m^{-1})	Reference
1	$Fe_{46}Co_{35}Ni_{19}$	Chemical reduction	132	49165	[15]
2	$Fe_{50}Co_{30}Ni_{20}$	Chemical reduction	161	29515	[16]
3	$Fe_{40}Co_{30}Ni_{30}$	Mechanical alloying	146	4300	[17]
4	$Fe_{45}Co_{45}Ni_{10}$	Mechanical alloying	186	2546	[18]
5	$Fe_{46}Co_{34}Ni_{20}$	Mechanical alloying	169	3300	[19]
6	FeCoNi	Vacuum melting	149	121	[20]
7	FeCoNi	Vacuum melting	164	55.9	[21]

Note: M_s is the saturation magnetization; H_c is the coercivity.

At present, the preparation methods of FeCoNi MEA are mainly vacuum arc melting and vacuum induction melting [41–44]. Some challenges such as demanding raw materials, high preparation costs, and cumbersome processing proced-

✉ Corresponding authors: Qing Zhao E-mail: zhaoq@smm.neu.edu.cn; Mengjie Tao E-mail: 2310655@stu.neu.edu.cn

ures greatly limit the industrial application of FeCoNi MEA. The liquid-phase method for preparing precursor powders not only addresses resource waste and environmental pollution caused by waste materials, transforming waste into valuable resources, but also enables the high-value utilization of such waste [39–40]. Typical preparation methods in the liquid-phase approach include hydrothermal method, sol–gel method, and chemical co-precipitation method. The hydrothermal method is a novel technique developed in recent years for synthesizing ultrafine powders. This method involves using an aqueous solution as the reaction system within a specially designed closed reactor (autoclave), where the system is heated to critical temperatures (or near critical temperatures) to create a high-pressure environment that facilitates inorganic synthesis and material preparation. Compared to other powder preparation methods, products obtained via the hydrothermal method typically exhibit well-developed crystal grains, small and uniformly distributed particle sizes, and mild particle aggregation. However, the hydrothermal method has its drawbacks, as it requires high temperature and pressure, leading to a strong dependence on production equipment, and it generally can only prepare oxide powders [25–26]. The sol–gel method involves the preparation of a homogeneous sol through the water hydrolysis of metal alkoxides or inorganic salt coordination, followed by the addition of solvents, catalysts, chelating agents, etc., to form a non-flowing aqueous sol, which is then converted into a uniform gel under certain conditions. After removing organic substances, water, and acid radicals, the gel undergoes drying and heat treatment to obtain the powder materials. The advantages of the sol–gel method include easy process control, the feasibility of doping, and its suitability for preparing small-sized, narrowly distributed, and chemically active amorphous materials of single or multi-component mixtures. However, its disadvantages include high raw material costs, lengthy reaction times, poor sinterability of microparticles, large shrinkage during drying that can lead to aggregation, and the presence of residual impurities such as carbon in the product [29–30]. The chemical co-precipitation method is an effective and commonly used technique for preparing powder materials. It involves adding a precipitating agent to a solution containing one or more soluble salt ions, allowing for a hydrolysis reaction to occur that forms insoluble hydroxides, hydrated oxides, or salts which then precipitate from the solution. Subsequently, any existing anions in the solvent or solution are washed away, and through hydrothermal treatment or dehydration, the powder materials can be obtained. The chemical co-precipitation method boasts advantages such as simplicity, low cost, short reaction times, low reaction temperatures, and ease of industrial scale-up. However, its disadvantages include lower product purity, difficulties in washing and filtering the precipitate, and a higher tendency for the resulting microparticles to aggregate [33–34].

In this study, a Fe^{3+}–Co^{2+}–Ni^{2+} solution was prepared through nitrates, which was employed to prepare FeCoNi MEA. To achieve composition uniformity and avoid element segregation, the sol–gel and co-precipitation methods were used to prepare precursors, respectively. Moreover, carbon thermal and hydrogen reductions were conducted to prepare FeCoNi MEA, and the phase composition, distribution of elements, and magnetic properties of reduction products were investigated.

2. Experimental

2.1. Theoretical calculation

The phase formation law of medium entropy alloys is almost consistent with that of high entropy alloys, and the inference formula of relevant parameters is used to predict the phase formation law of FeCoNi MEAs [45–51]. The related thermodynamic parameters of FeCoNi MEAs are shown in Table 2, and the atomic radius, melting point and valence electron concentration of Fe, Co and Ni in Table 3. The calculation data can infer that FeCoNi MEAs can form a single face centered cubic (FCC) structure solid solution.

Table 2. Related thermodynamic parameters of FeCoNi medium entropy alloy

δ / %	ΔH_{mix} / (kJ·mol^{-1})	ΔS_{mix} / (J·K^{-1}·mol^{-1})	T_m / °C	Ω	VEC
0.9	−1.33	9.15	1495.3	1.2	9

Note: δ is the difference in atomic radius (%), ΔH_{mix} is the enthalpy of mixing (kJ·mol^{-1}), ΔS_{mix} is the entropy of mixing (J·K^{-1}·mol^{-1}), T_m is the theoretical melting point of the alloy (°C), Ω is the parameter point, VEC is the valence electron concentration of the alloy.

Table 3. Atomic radius, melting point, and valence electron concentration of Fe, Co, and Ni

Element	Atomic radius / Å	Melting point / °C	VEC
Fe	1.27	1538	8
Co	1.25	1495	9
Ni	1.25	1453	10

2.2. Materials

The following analytical reagents were used: Fe$(NO_3)_3$·$9H_2O$ (≥99.0%), Co$(NO_3)_2$·$6H_2O$ (≥99.0%), Ni$(NO_3)_2$·$6H_2O$ (≥99.0%), NaOH (≥99.0%), $C_6H_8O_7$ (≥99.0%), NH_3·H_2O (25wt%), N_2 (≥99.9%), and H_2 (≥99.9%). All reagents were purchased from National Pharmaceutical (Shanghai Trial) Co., Ltd. The deionized water used in this experiment was self-made in the laboratory by the UPTA-10 ultra-pure water machine.

2.3. Preparation of precursor

2.3.1. Sol–gel method

A certain amount of nitrates (Fe$(NO_3)_3$·$9H_2O$, Co$(NO_3)_3$·$6H_2O$, Ni$(NO_3)_3$·$6H_2O$) were weighed in an equal molar ratio and dissolved in a deionized water. The solution was stirred at a speed of 200 r·min^{-1} and maintained during

the whole process to make the solutes completely dissolve. A prepared citric acid solution was slowly added to the Fe^{3+}–Co^{2+}–Ni^{2+} solution, after which the $NH_3{\cdot}H_2O$ was employed to adjust the pH value of the solution to 8. The mixed solution was heated in a 90°C water bath for 8 h to obtain a sol. The sol was dried in a drying oven at 110°C for 24 h to obtain a gel, i.e., the precursor.

2.3.2. Co-precipitation method

A certain amount of nitrates ($Fe(NO_3)_3{\cdot}9H_2O$, $Co(NO_3)_3{\cdot}6H_2O$, $Ni(NO_3)_3{\cdot}6H_2O$) were weighed in an equal molar ratio and dissolved in deionized water. The solution was stirred at a speed of 200 $r{\cdot}min^{-1}$ and maintained during the whole process to make solutes completely dissolve. 2 $mol{\cdot}L^{-1}$ NaOH solution was prepared and slowly dripped into the solution using a peristaltic pump until the pH value reached 10. The solution was aged at room temperature for 10 h, and the precipitates were repeatedly washed and separated by vacuum filtration. The samples were dried in a drying oven at 100°C for 10 h to obtain a precursor.

2.4. Preparation of FeCoNi MEA

2.4.1. Carbothermal reduction method

The activated carbon particles and precursor were mechanically mixed. The used activated carbon was 1.5 times the theoretical calculation amount. The mixed powder was added to a graphite crucible and heated to 1500°C in a high-temperature atmosphere furnace (XNF-OL8600). After 3 h, argon gas was introduced to protect the products from oxidizing. The heating rate was 3.5°C·min^{-1}. The cooling method was quenching. The cooling rate was approximately 1500°C·min^{-1}.

2.4.2. Hydrogen reduction method

The precursor was added in a corundum crucible, and placed in a high-temperature atmosphere furnace. When samples were heated to 1500°C, hydrogen gas was introduced with a flow rate of 500 mL·min^{-1} for 3 h, and argon gas was injected after the hydrogen reduction process. The sample was cooled to room temperature in the furnace. The heating rate was 3.5°C·min^{-1}. The cooling method was quenching. The cooling rate was approximately 1500°C·min^{-1}.

2.5. Characterization

2.5.1. Phase composition

The phase composition of the precursor and reduction product was determined using an X-ray diffractometer (XRD, D8 Advance, Brook Technology, Germany) with a continuous scanning device using Cu K_α radiation at 30 mA/40 kV, a scanning speed is 6°·min^{-1}, and a 2θ range of 10°–90°. The results were analyzed using JADE 9.0 software based on the International Centre for Diffraction Data (ICDD) powder diffraction database (PDF-2009).

The phase structure of the precursor prepared by the sol–gel method was detected using Fourier transform infrared spectroscopy (FT-IR, Thermo Scientific Nicolet iS20, Thermo Fisher Technologies, America) in the spectral range of 1100–2200 cm^{-1}, the number of scans was 32, and the resolution was 4 cm^{-1}.

2.5.2. Morphology

The morphology of precursor and reduction product was observed using scanning electron microscopy (SEM, ZEISS GeminiSEM 300, Carl Zeiss Optics Ltd., Germany). The types and contents of elements in specific micro-regions of samples were detected using an X-ray energy dispersive spectrometer (EDS).

2.5.3. Decomposition behavior

Thermogravimetric–differential scanning calorimetry (TG–DSC) analysis was carried out using a high-temperature synchronous thermal analyzer (STA409CD, Naichi Instrument Manufacturing Co., Ltd. Germany) in the argon atmosphere to investigate the decomposition behaviors of precursor. The heating ranges were 40–1000°C with a rate of 10°C·min^{-1} for samples prepared by sol–gel and co-precipitation methods, respectively.

2.5.4. Magnetic performance

The magnetic properties of reduction products were tested using the physical property measurement system (PPMS) DynaCool system developed by Quantum Design USA. In the normal temperature and pre-air environment, the magnetic field was applied within a range of ±2 T. The hysteresis curves at room temperature were measured, and the coercive force and saturation strength of the samples were characterized.

3. Results and discussion

3.1. Preparation of precursor

3.1.1. Sol–gel method

The product prepared by the sol–gel method was ground and analyzed by FT-IR and SEM-EDS, and the results are provided in Fig. 1, and the energy spectrum analysis of precursor prepared by sol–gel method as shown in Table 4. It can be seen from the FT-IR pattern (Fig. 1(a)), that the absorption band near the carboxylic acid group 1757 cm^{-1} partially disappears, and two absorption bands near 1617 cm^{-1} and 1353 cm^{-1} replace it, which was attributed to the R–COO group generation by ionization. It was speculated that the citric acid complexed with metal ions forming citrate in the precursor.

The SEM image of the product prepared by the sol–gel method is shown in Fig. 1(b). Some spherical and irregular particles can be observed in the image. To clarify the chemical composition and element, EDS analysis was performed in Fig. 1(c). Results indicated that the sample mainly contained Fe, Co, Ni, O, and C. The atomic ratio of Fe, Co, Ni was close to 1:1:1, which proved that a precursor of FeCoNi MEA was prepared by the sol–gel method. Moreover, little N was detected in the sample, which may be adsorbed by the sol.

3.1.2. Co-precipitation method

XRD analysis was performed on the samples prepared by the co-precipitation method. As shown in Fig. 2(a), diffraction peaks of $Fe(OH)_3$, $Co(OH)_2$, and $Ni(OH)_2$ cannot

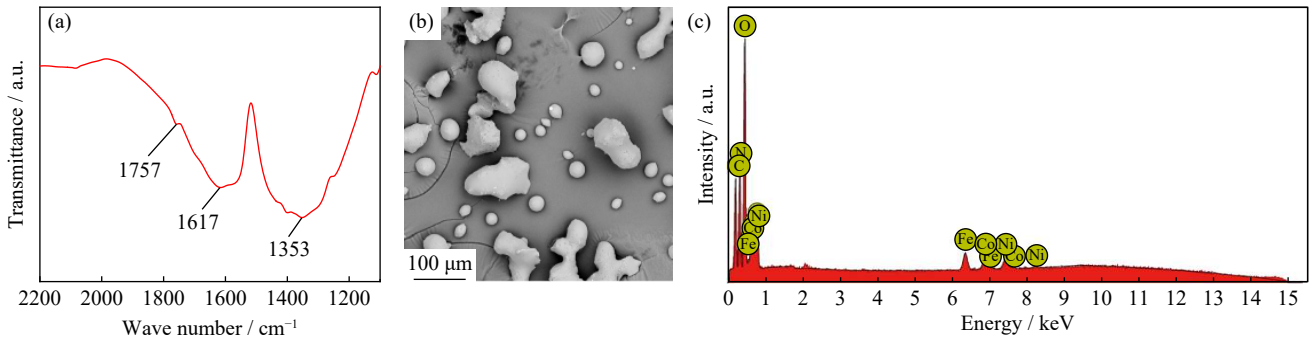

Fig. 1. (a) FT-IR pattern, (b) SEM image, and (c) EDS analysis of the precursor prepared by sol–gel method.

Table 4. Energy spectrum analysis of the precursor prepared by sol–gel method.

Element	Weight percent / %	Atomic percent / %
O	66.55	51.60
N	13.77	9.35
C	7.23	4.21
Fe	4.50	12.18
Ni	4.15	11.81
Co	3.80	10.85

be detected in the sample. SEM-EDS analysis was employed for further determination of the phase composition. It can be seen from Fig. 2(b) that the precipitates showed an irregular fragmented shape. EDS results in Fig. 2(c) indicated that the sample mainly contained Fe, Co, Ni, and O, and the energy spectrum analysis of precursor by chemical co-precipitation method as shown in Table 5. The atomic ratio of Fe, Co, Ni was close to 1:1:1. On the basis of these findings, it was obtained that the precursor prepared by co-precipitation was not in the form of a hydroxide crystal, which might be an amorphous composite of hydroxides or hydroxyl oxides.

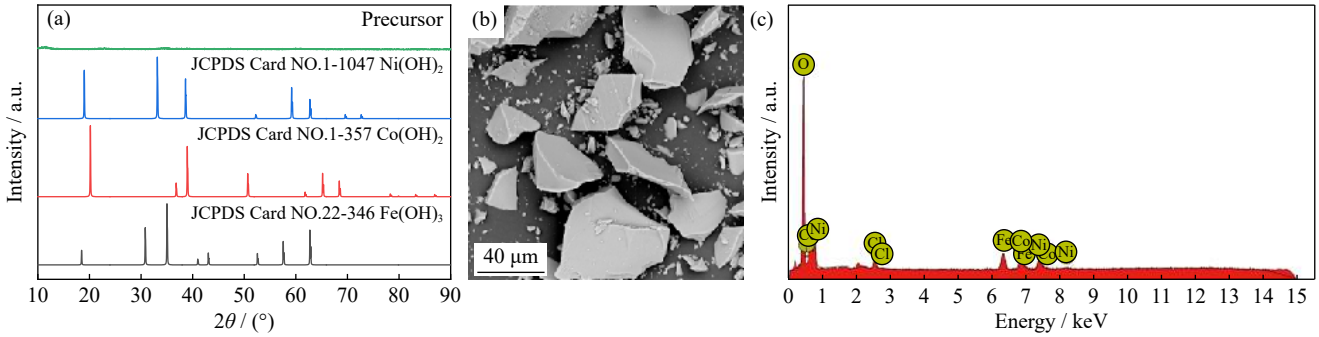

Fig. 2. (a) XRD pattern (b) SEM image, and (c) EDS analysis of the product prepared by co-precipitation.

3.2. Decomposition and reduction behaviors of precursors

3.2.1. Decomposition behavior

To understand the thermal decomposition behavior of the precursors, TG–DSC analysis was conducted showing the results in Fig. 3. It can be seen from Fig. 3(a) that the weight of the sample prepared by the sol–gel method decreased with temperature until 548°C. No notable changes were seen after the temperature exceeded 548°C. The first significant mass loss appeared at around 248°C. The mass change was mainly caused by the decomposition of citrate. The second significant mass loss appeared at around 548°C. The mass change was mainly caused by the decomposition of nitrates. Fig. 3(b) shows the TG–DSC curve of the sample prepared by the co-precipitation method. Before 871°C, the weight of the precursor continuously decreased with temperature. Few changes can be observed after the temperature exceeds 871°C. The first significant mass loss appeared at around 234°C. The mass change was mainly caused by the decomposition of hydroxides. The second significant mass loss appeared at around 871°C. The mass change was mainly caused by the decomposition of residual nitrates.

Table 5. Energy spectrum analysis of precursor prepared by chemical co-precipitation

Element	Weight percent / %	Atomic percent / %
O	41.63	71.54
Ni	20.11	9.42
Fe	17.87	8.80
Co	18.04	8.42
Cl	2.35	1.82

3.2.2. Reduction behavior

Fe–Co–Ni oxides can be generated during the heating process of precursors. The Gibbs free energy–temperature (ΔG–T) diagrams of chemical reactions occurring during carbothermic and hydrogen reductions were drawn based on FactSage software, as shown in Fig. 4. The results showed that the Fe–Co–Ni oxides could be reduced by C when the temperature was higher than 700°C. Similarly, zero-valence Fe, Co, and Ni could form at around 600°C during a hydrogen reduction process. An isothermal liquidus diagram of the

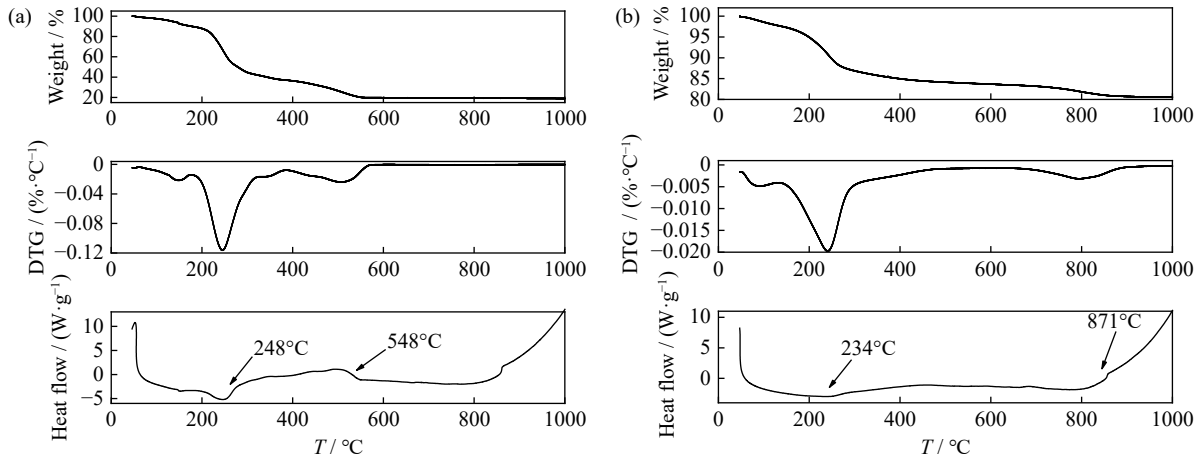

Fig. 3. TG–DSC curves of the precursors prepared by (a) sol–gel and (b) co-precipitation methods. DTG: Derivative thermogravimetry.

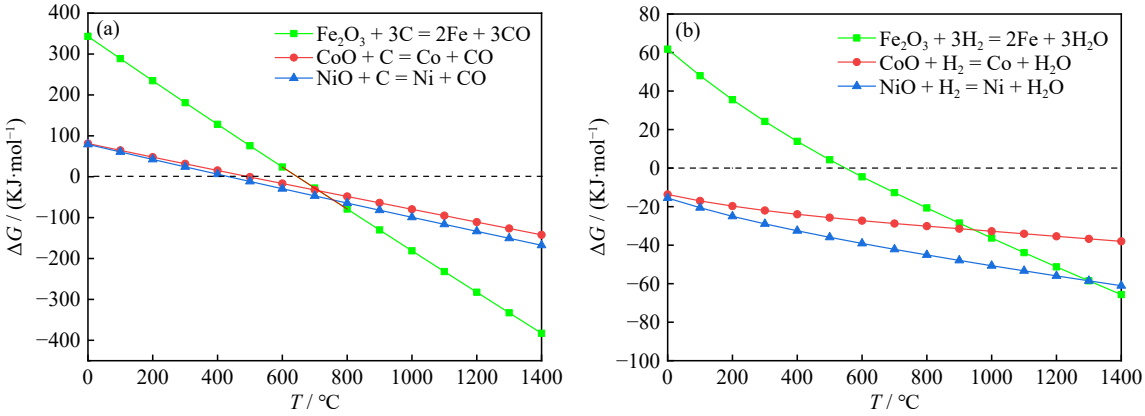

Fig. 4. ΔG–T diagrams of chemical reactions occurring during (a) carbothermic and (b) hydrogen reductions.

Fe–Co–Ni ternary system was drawn based on FactSage software, which was shown in Fig. 5. The results showed that the melting point of an equiatomic FeCoNi system was 1469°C. To prepare a homogeneous FeCoNi MEA, the temperatures for carbothermal and hydrogen reductions of precursors were chosen to be 1500°C in the current work.

3.3. Preparation of FeCoNi MEA

3.3.1. Carbothermal reduction

Carbothermal reduction was carried out to the precursors prepared by sol–gel and co-precipitation methods. The phase composition of the product prepared by the sol–gel method followed by carbothermal reduction was analyzed by XRD, showing the results in Fig. 6(a). It was found that the diffraction peaks of the sample shifted to the right a little compared with that of the FeCoNi. An explanation of this finding is proposed that some carbon doped in the product in the carbothermal reduction process, resulting in a slight shift of the peak position. To verify this view, the product was detected by SEM analysis (Fig. 6(b)). About 9.16wt% carbon element was detected in the FeCoNi MEA (Table 6), and the black coarse and fine rod-like phases in Fig. 6(b) were verified to be carbon. It explained the conjecture of diffraction peak shift. Furthermore, the product contains a small amount of oxygen element meaning the carbothermal reduction was incomplete.

XRD patterns and SEM analysis of the product prepared by co-precipitation followed by carbothermal reduction are showed in Fig. 7. It can be seen from Fig. 7(a) that the diffraction peak position was similar to that of the sample prepared by the sol–gel method followed by carbothermal reduction (Fig. 6(a)), which shifted to the right a little as well. However, the relative intensity of diffraction peaks of the two products were different. This phenomenon might be caused by the difference between the preparation methods of the precursor. SEM results indicated that some carbon doped in the

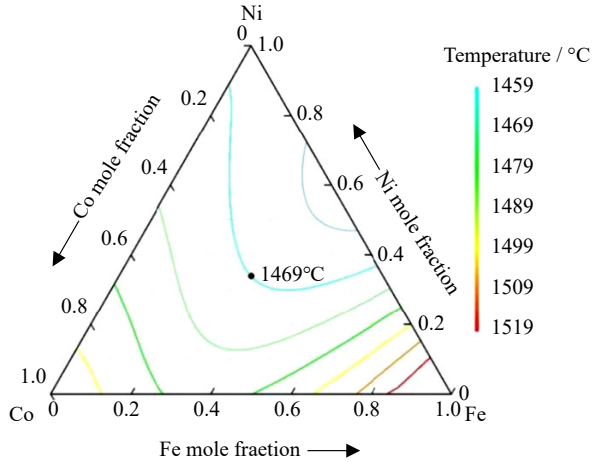

Fig. 5. Isothermal liquidus diagram of Fe–Co–Ni ternary system.

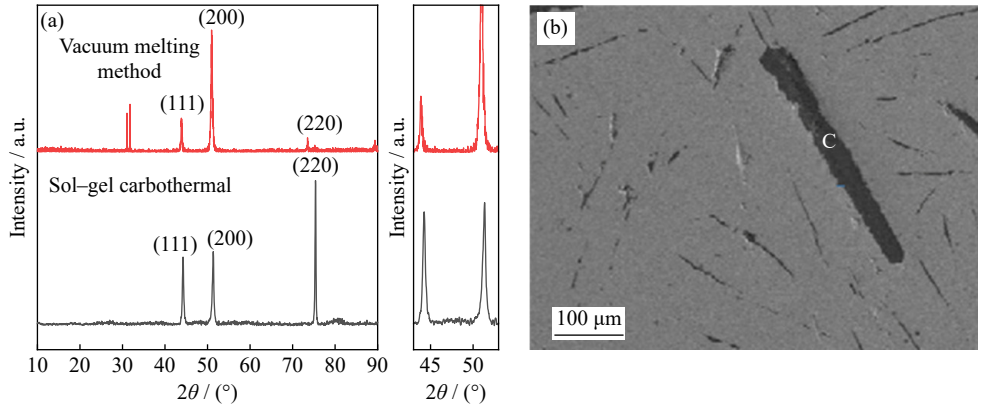

Fig. 6. (a) XRD patterns and (b) SEM image of the product prepared by the sol–gel method followed by carbothermal reduction.

Table 6. Energy spectrum analysis of FeCoNi MEA prepared by the sol–gel method followed by carbothermal reduction wt%

Fe	Co	Ni	C	O	N
27.20	29.88	27.20	9.16	4.11	2.45

FeCoNi MEA, and the carbothermal reduction did not go complete (Table 7).

3.3.2. Hydrogen reduction

Hydrogen reduction was carried out to the precursors prepared by co-precipitation methods. The phase composition of

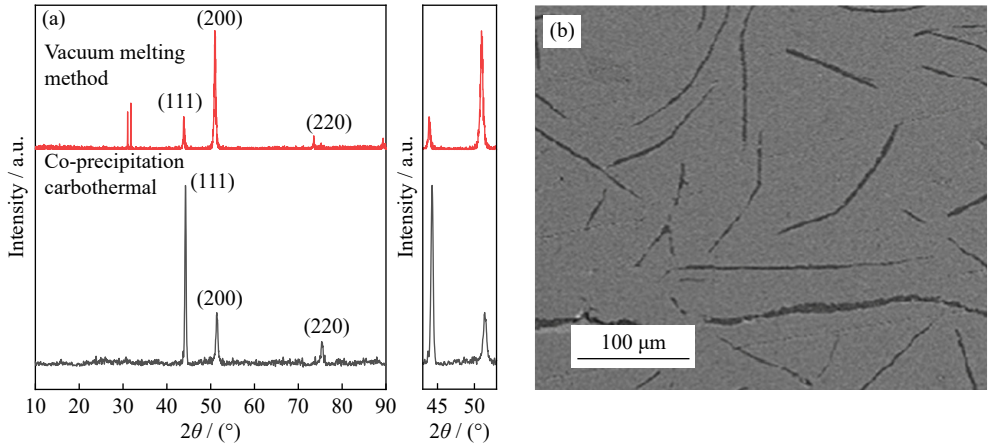

Fig. 7. (a) XRD patterns and (b) SEM image of the product prepared by co-precipitation followed by carbothermal reduction.

Table 7. Energy spectrum analysis of FeCoNi medium entropy alloy prepared by co-precipitation followed by carbothermal reduction wt%

Fe	Co	Ni	C	O
30.14	30.36	29.47	6.15	3.88

the product prepared by the co-precipitation followed by hydrogen reduction was analyzed by XRD, showing the results in Fig. 8. It can be seen in Fig. 8 that the diffraction peak position of the sample was consistent with the FeCoNi, meaning the target product was prepared by this route.

Fig. 9(a) shows an SEM image of the product prepared by co-precipitation followed by hydrogen reduction. As shown in Fig. 9(a), the prepared product was a homogeneous phase containing some small pores. The reason was attributed to the bubbles generated during the hydrogen reduction process and were sealed in the sample after cooling. EDS analysis was used to investigate the elemental distribution of the product showing the result in Fig. 9(b), and the energy spectrum analysis of FeCoNi medium entropy alloy prepared by co-precipitation followed by hydrogen reduction as shown in Table 8. Results indicated that the atomic ratio of Fe, Co, and Ni was close to 1:1:1, and the element distribution was uniform. The absence of oxygen in the product proves that the reduction was complete. The studied preparation method of precursor did not significantly affect the product of hydrogen reduction. On the basis of these findings, the FeCoNi MEA can be prepared by the hydrogen reduction method.

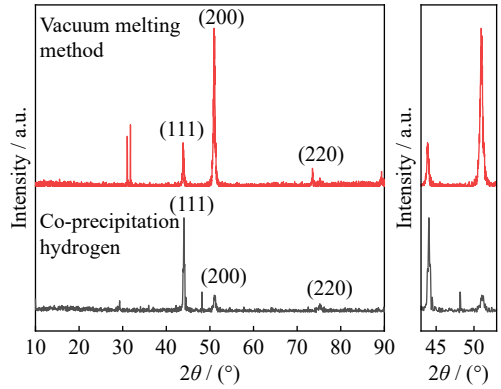

Fig. 8. XRD patterns of the product prepared by co-precipitation followed by hydrogen reduction.

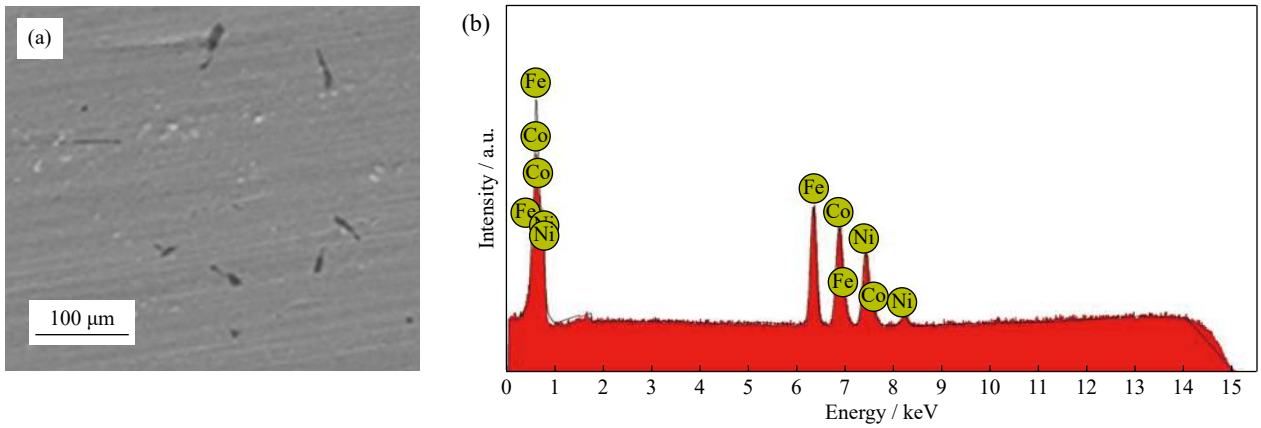

Fig. 9. (a) SEM image and (b) EDS result of the product prepared by co-precipitation followed by hydrogen reduction.

Table 8. Energy spectrum analysis of FeCoNi MEA prepared by co-precipitation followed by hydrogen reduction

Element	Weight percent / %	Atomic percent / %
Fe	33.34	34.51
Co	33.33	32.68
Ni	33.33	32.81

3.4. Magnetic properties of FeCoNi MEA

The magnetic properties of products prepared by the sol–gel/co-precipitation followed by carbothermal reduction were tested using PPMS, and the results were shown in Fig. 10. Results showed that the saturation magnetization of the sample prepared by sol–gel followed by carbothermal reduction was 152.7 emu·g^{-1}, and the coercivity was 275.1 A·m^{-1}. As for the sample prepared by the co-precipitation followed by carbothermal reduction, the saturation magnetization and coercivity were 147.7 emu·g^{-1} and 210.7 A·m^{-1}, respectively. The two products exhibited a relatively weak magnetic performance. The main reason was attributed to the existence of the carbon phase. The phase interface in the alloy greatly hindered the movement of the magnetic domain wall, causing a large coercivity.

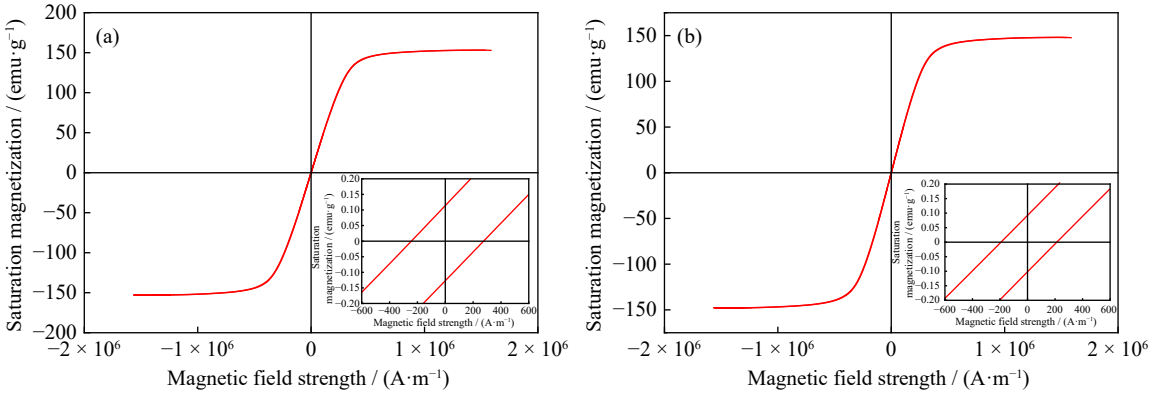

Fig. 10. Hysteresis loops diagram of products prepared by (a) sol–gel method and (b) co-precipitation followed by carbothermal reduction.

The magnetic properties of the FeCoNi medium-entropy alloy prepared by co-precipitation followed by hydrogen reduction method were tested using PPMS, and the results are shown in Fig. 11. From Fig. 11, it can be observed that the saturation magnetization of the FeCoNi medium-entropy alloy prepared by co-precipitation hydrogen reduction method is 155.8 emu·g^{-1}, with a coercivity of 113.5 A·m^{-1}, indicating good soft magnetic properties.

Furthermore, the saturation magnetization of the FeCoNi medium-entropy alloy prepared by vacuum arc melting was measured using PPMS, yielding a value of 155.9 emu·g^{-1} and a coercivity of 109.6 A·m^{-1}. The saturation magnetization and coercivity of FeCoNi medium-entropy alloys prepared using the sol–gel thermochemical reduction method, chemical co-precipitation thermochemical reduction method, and

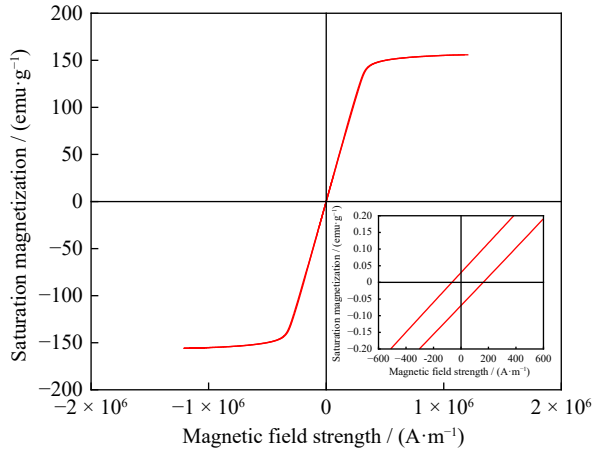

Fig. 11. Hysteresis loops diagram of the product prepared by co-precipitation followed by hydrogen reduction.

chemical co-precipitation hydrogen reduction method are summarized in Table 9. It can be concluded that the coercivity of the FeCoNi medium-entropy alloy prepared by hydrogen reduction is lower than that of the alloy prepared by thermochemical reduction, and it has a coercivity similar to that of the vacuum arc melting method, indicating better soft magnetic properties.

Table 9. Summary of saturation magnetization and coercivity of different preparation methods

Method	M_s / (emu·g^{-1})	H_c / (A·m^{-1})
Sol–gel thermochemical reduction method	152.7	275.1
Chemical co-precipitation thermochemical reduction method	147.7	210.7
Chemical co-precipitation hydrogen reduction method	155.8	113.5
Vacuum arc melting method	155.9	109.6

4. Conclusions

The focus of this article is experimental research that explores a novel method for producing medium entropy alloys composed of FeCoNi. The process involved a combination of hydrometallurgy and pyrometallurgy, utilizing solutions containing Fe, Co, and Ni as the primary materials. According to the various conditions tested, the results are summarized as follows.

(1) Both the sol–gel method and the co-precipitation method can be utilized to produce amorphous FeCoNi medium entropy alloy precursors with atomic ratios of Fe, Co, and Ni that are nearly 1:1:1. It was speculated that the sol–gel method yields a complex citrate precursor, while the co-precipitation method produces a complex hydroxide or hydroxyl oxide precursor.

(2) The decomposition temperature of the FeCoNi precursor was determined by TG–DSC analysis. Based on FactSage software, the ΔG–T diagrams of chemical reactions occurring during carbothermic and hydrogen reductions and the isothermal liquidus diagram of the Fe–Co–Ni ternary system were drawn. As a result, it was determined that the optimal reaction temperature for the preparation of entropy alloy in FeCoNi using the carbon thermal reduction method and hydrogen reduction method was 1500°C.

(3) Two preparation methods, carbothermal reduction and hydrogen reduction, have been explored. At the same reaction temperature, the carbothermal reduction was incomplete. The residual carbon and oxides in the carbothermal reduction products also cause diffraction peaks to shift. The hydrogen reduction method can completely reduce the precursor. The FeCoNi MEA can be prepared by the hydrogen reduction method.

(4) The FeCoNi medium entropy alloy, prepared using hydrogen reduction, has a saturation magnetization of 155.8 emu·g^{-1} and a coercivity of 113.5 A·m^{-1}. These magnetic properties were comparable to the ones obtained from vacuum arc melting. Moreover, it was superior to the magnetic properties of the FeCoNi medium entropy alloy that was prepared using carbothermal reduction.

Acknowledgements

This work was financially supported by the National Natural Science Foundation of China (Nos. 52074078 and 52374327), the Applied Fundamental Research Program of Liaoning Province, China (No. 2023JH2/101600002), the Liaoning Provincial Natural Science Foundation, China (No. 2022-YQ-09), the Shenyang Young Middle-Aged Scientific and Technological Innovation Talent Support Program, China (No. RC220491), the Liaoning Province Steel Industry-University-Research Innovation Alliance Cooperation Project of Bensteel Group, China (No. KJBLM202202), and the Fundamental Research Funds for the Central Universities, China (Nos. N2201023 and N2325009).

Conflict of Interest

All authors do not have competing interests to declare.

References

[1] J.W. Yeh, S.K. Chen, S.J. Lin, *et al*., Nanostructured high-entropy alloys with multiple principal elements: Novel alloy design concepts and outcomes, *Adv. Eng. Mater.*, 6(2004), No. 5, p. 299.

[2] W.R. Zhang, P.K. Liaw, and Y. Zhang, Science and technology in high-entropy alloys, *Sci. China Mater.*, 61(2018), No. 1, p. 2.

[3] J. Chen, X.Y. Zhou, W.L. Wang, *et al*., A review on fundamental of high entropy alloys with promising high–temperature properties, *J. Alloys Compd.*, 760(2018), p. 15.

[4] A. Takeuchi, Recent progress in alloy designs for high-entropy crystalline and glassy alloys, *J. Jpn. Soc. Powder Powder Metall.*, 63(2016), No. 4, p. 209.

[5] D.L. Beke and G. Erdélyi, On the diffusion in high-entropy alloys, *Mater. Lett.*, 164(2016), No. 164, p. 111.

[6] B. Gludovatz, A. Hohenwarter, K.V.S. Thurston, *et al*., Exceptional damage-tolerance of a medium-entropy alloy CrCoNi at cryogenic temperatures, *Nat. Commun.*, 7(2016), art. No. 10602.

[7] Z. Wu, H. Bei, G.M. Pharr, and E.P. George, Temperature dependence of the mechanical properties of equiatomic solid solution alloys with face-centered cubic crystal structures, *Acta Mater.*, 81(2014), p. 428.

[8] G. Laplanche, A. Kostka, C. Reinhart, J. Hunfeld, G. Eggeler, and E.P. George, Reasons for the superior mechanical properties of medium-entropy CrCoNi compared to high-entropy CrMnFeCoNi, *Acta Mater.*, 128(2017), p. 292.

[9] R.P. Zhang, S.T. Zhao, J. Ding, *et al*., Short-range order and its impact on the CrCoNi medium-entropy alloy, *Nature*, 581(2020), No. 7808, p. 283.

[10] H. Song, D.G. Kim, D.W. Kim, *et al*., Effects of strain rate on room- and cryogenic-temperature compressive properties in metastable $V_{10}Cr_{10}Fe_{45}Co_{35}$ high-entropy alloy, *Sci. Rep.*, 9(2019), No. 1, art. No. 6163.

[11] Z. Cheng, S.Z. Wang, G.L. Wu, J.H. Gao, X.S. Yang, and H.H. Wu, Tribological properties of high-entropy alloys: A review, *Int. J. Miner. Metall. Mater.*, 29(2022), No. 3, p. 389.

[12] J.L. Chen, Z.X. Feng, J.H. Yi, and J. Yang, Effect of low tem-

perature rolling on mechanical properties and corrosion resistance of CrCoNi medium entropy alloy, *Mater. Res. Express*, 9(2022), No. 1, art. No. 016502.
[13] X. L. An, *Design, Microstructure and Properties of CoNiFe-based Ternary Medium Entropy Alloy with Face Centered Cubic* [Dissertation], Southeast University, Nanjing, 2020, p. 1.
[14] H. Zhou, *Effect of Plastic Deformation on Microstructure and Properties of CoCrFeNi High-entropy Alloy* [Dissertation], Southeast University, Nanjing, 2020, p. 12.
[15] H.Q. Wu, D.M. Xu, Q. Wang, Q.Y. Wang, G.Q. Su, and X.W. Wei, Composition-controlled synthesis, structure and magnetic properties of ternary $Fe_xCoyNi_{100-x-y}$ alloys attached on carbon nanotubes, *J. Alloys Compd.*, 463(2008), No. 1–2, p. 78.
[16] K. Chokprasombat, S. Pinitsoontorn, and S. Maensiri, Effects of Ni content on nanocrystalline Fe–Co–Ni ternary alloys synthesized by a chemical reduction method, *J. Magn. Magn. Mater.*, 405(2016), p. 174.
[17] T.V. Jayaraman, A. Rathi, and G.V. Thotakura, Evaluation of the suitability of $Fe_{40}Co_{30}Ni_{30}$ as a precursor for Fe-rich Fe-CoNi-based high-entropy semi-hard magnets, *Intermetallics*, 119(2020), art. No. 106715.
[18] H. Ahmadian Baghbaderani, S. Sharafi, and M. Delshad Chermahini, Investigation of nanostructure formation mechanism and magnetic properties in $Fe_{45}Co_{45}Ni_{10}$ system synthesized by mechanical alloying, *Powder Technol.*, 230(2012), p. 241.
[19] G.V. Thotakura, A. Rathi, and T.V. Jayaraman, Structure and magnetic properties of mechanically alloyed nanocrystalline Fe–46at.%Co–34at.%Ni–20at.% alloy powder from cryogenic to elevated temperatures, *Appl. Phys. A*, 125(2019), No. 4, art. No. 235.
[20] T.T. Zuo, *Microstructure and Properties of Co–Fe–Ni Magnetic High-Entropy Alloy* [Dissertation], University of Science and Technology Beijing, Beijing, 2017, p. 3.
[21] Z. Li, *Magnetic Properties and Microstructure of FeCoNiM_x (M=AlCu, AlMn, AlSi, and MnSi) High-entropy Alloys* [Dissertation], Shanghai University, Shanghai, 2019, p.15.
[22] A. Rathi, V.M. Meka, and T.V. Jayaraman, Synthesis of nanocrystalline equiatomic nickel–cobalt–iron alloy powders by mechanical alloying and their structural and magnetic characterization, *J. Magn. Magn. Mater.*, 469(2019), p. 467.
[23] W. Li, P. Liu, and P.K. Liaw, Microstructures and properties of high-entropy alloy films and coatings: A review, *Mater. Res. Lett.*, 6(2018), No. 4, p. 199.
[24] H.T. Luo, *Regenerated Silicate Material Using Waste Concrete-clay Brick by Hydrothermal Synthesis* [Dissertation], Dalian University of Technology, Dalian, 2020, p. 20.
[25] K.V. Raun, L.F. Lundegaard, J. Chevallier, *et al*., Deactivation behavior of an iron-molybdate catalyst during selective oxidation of methanol to formaldehyde, *Catal. Sci. Technol.*, 8(2018), No. 18, p. 4626.
[26] K.V. Raun, L.F. Lundegaard, P. Beato, *et al*., Stability of iron–molybdate catalysts for selective oxidation of methanol to formaldehyde: Influence of preparation method, *Catal. Lett.*, 150(2020), No. 5, p. 1434.
[27] A.E. Ameh, O.O. Fatoba, N. Musyoka, B. Louis, and L. Petrik, Transformation of fly ash based nanosilica extract to BEA zeolite and its durability in hot liquid, *Microporous Mesoporous Mater.*, 305(2020), art. No. 110332.
[28] E. Muchuweni, T.S. Sathiaraj, and H. Nyakotyo, Hydrothermal synthesis of ZnO nanowires on rf sputtered Ga and Al Co-doped ZnO thin films for solar cell application, *J. Alloys Compd.*, 721(2017), p. 45.
[29] D. Cao, *Study on Preparation of High Purity Alumina Powder from Waste Aluminum* [Dissertation], Dalian Jiaotong University, Dalian, 2014, p. 15.
[30] S. Carstens and D. Enke, Investigation of the formation process of highly porous α-Al_2O_3 via citric acid-assisted sol–gel synthesis, *J. Eur. Ceram. Soc*, 39(2019), No. 7, p. 2493.
[31] G.T.K. Fey, R.F. Shiu, V. Subramanian, J.G. Chen, and C.L. Chen, $LiNi_{0.8}Co_{0.2}O_2$ cathode materials synthesized by the maleic acid assisted sol–gel method for lithium batteries, *J. Power Sources*, 103(2002), No. 2, p. 265.
[32] S.M. Sajjadi, M. Haghighi, A.A. Eslami, and F. Rahmani, Hydrogen production via CO_2-reforming of methane over Cu and Co doped Ni/Al_2O_3 nanocatalyst: Impregnation versus sol–gel method and effect of process conditions and promoter, *J. Sol–Gel Sci. Technol*., 67(2013), No. 3, p. 601.
[33] L. Liu, *The Manufacture of Lithium Manganses Iron Phosphate Precursor Using Low-grade Manganese Ore and Crap Iron* [Dissertation], Northeastern University, Shenyang, 2018, p. 31.
[34] V. Karimi, M. Asemi, and M. Ghanaatshoar, Improving photovoltaic properties of ZTO-based DSSCs using surface modification of Zn_2SnO_4 nanoparticles prepared by co-precipitation method, *Mater. Sci. Semicond. Process.*, 127(2021), art. No. 105664.
[35] S. Tillaoui, A. El Boubekri, A. Essoumhi, *et al*., Structural, magnetic, magnetocaloric properties and critical behavior of $La_{0.62}Nd_{0.05}Ba_{0.33}MnO_3$ elaborated by co-precipitation process, *Mater. Sci. Eng. B*, 266(2021), art. No. 115052.
[36] S.V.M. Goorabjavari, F. Golmohamadi, S. Haririmonfared, *et al*., Thermodynamic and anticancer properties of inorganic zinc oxide nanoparticles synthesized through co-precipitation method, *J. Mol. Liq.*, 330(2021), art. No. 115602.
[37] S. Akilandeswari, G. Rajesh, D. Govindarajan, K. Thirumalai, and M. Swaminathan, Efficacy of photoluminescence and photocatalytic properties of Mn doped ZrO_2 nanoparticles by facile precipitation method, *J. Mater. Sci. Mater. Electron.*, 29(2018), No. 21, p. 18258.
[38] K.J. Park, M.J. Choi, F. Maglia, *et al*., High-capacity concentration gradient $Li[Ni_{0.865}Co_{0.120}Al_{0.015}]O_2$ cathode for lithium-ion batteries, *Adv. Energy Mater.*, 8(2018), No. 19, art. No. 1703612.
[39] Y. Sun, J. Zhang, T. Li, and Q.J. Li, Experimental study on reduction Ni from stainless steel sludge, *Shanghai Met.*, 38(2016), No.2, p. 64.
[40] X.D. Zhang, S.L. Liang, B. Liu, X.J. Liu, and Z.L. Li, Study on preparation of Mn–Zn ferrite by waste dry battery and titanium dioxide waste acid, *Inorg. Chem. Ind*, 45(2013), No. 07, p. 44.
[41] Z. Wu, H. Bei, F. Otto, G.M. Pharr, and E.P. George, Recovery, recrystallization, grain growth and phase stability of a family of FCC-structured multi-component equiatomic solid solution alloys, *Intermetallics*, 46(2014), p. 131.
[42] C.H. Tsau, S.X. Lin, and C.H. Fang, Microstructures and corrosion behaviors of FeCoNi and CrFeCoNi equimolar alloys, *Mater. Chem. Phys.*, 186(2017), p. 534.
[43] H.W. Yao, J.W. Qiao, M. Gao, J. Hawk, S.G. Ma, and H.F. Zhou, MoNbTaV medium-entropy alloy, *Entropy*, 18(2016), No. 5, art. No. 189.
[44] B. Uzer, S. Picak, J. Liu, *et al*., On the mechanical response and microstructure evolution of NiCoCr single crystalline medium entropy alloys, *Mater. Res. Lett.*, 6(2018), No. 8, p. 442.
[45] Y. Zhang, Y.J. Zhou, J.P. Lin, G.L. Chen, and P.K. Liaw, Solid–solution phase formation rules for multi-component alloys, *Adv. Eng. Mater.*, 10(2008), No. 6, p. 534.
[46] J.W. Yeh, Y.L. Chen, S.J. Lin, and S.K. Chen, High-entropy alloys–A new era of exploitation, *Mater. Sci. Forum*, 560(2007), p. 1.
[47] A. Takeuchi and A. Inoue, Classification of bulk metallic glasses by atomic size difference, heat of mixing and period of constituent elements and its application to characterization of the main alloying element, *Mater. Trans.*, 46(2005), No. 12, p. 2817.
[48] Z. Tang, O.N. Senkov, C.M. Parish, *et al*., Tensile ductility of an AlCoCrFeNi multi-phase high-entropy alloy through hot iso-

static pressing (HIP) and homogenization, *Mater. Sci. Eng. A*, 647(2015), p. 229.

[49] J.C. Jiang and X.Y. Luo, High temperature oxidation behaviour of AlCuTiFeNiCr high-entropy alloy, *Adv. Mater. Res*., 652–654(2013), p. 1115.

[50] X. Yang and Y. Zhang, Prediction of high-entropy stabilized solid-solution in multi-component alloys, *Mater. Chem. Phys.*, 132(2012), No. 2–3, p. 233.

[51] S. Guo, C. Ng, J. Lu, and C.T. Liu, Effect of valence electron concentration on stability of fcc or bcc phase in high entropy alloys, *J. Appl. Phys.*, 109(2011), No. 10, art. No. 103505.